

BL28B2

White beam X-ray Diffraction

1. Introduction

BL28B2 is dedicated to multiple techniques in several fields. It is a bending magnet beamline that uses white X-rays from a bending-magnet source without passing through any optical devices. Techniques include (1) X-ray diffraction, (2) dispersive-type time-resolved X-ray absorption fine structures (DXAFS), (3) microbeam radiation therapy (MRT), and (4) X-ray imaging. The beamline supports various experiments such as biological functional imaging with small animals, fundamental research for radiation therapy, evaluation of structural materials using white X-ray diffraction imaging, observations of dynamic structural changes during chemical reaction processes in catalysis and fuel-cell batteries using DXAFS, and three-dimensional observations of metallic objects using high-energy X-ray microtomography. To improve measurement techniques using this beamline, research and development of experimental techniques and instruments were conducted in FY2019. This report describes the main activities.

2. Beamline upgrades

2-1. Diffraction

In BL28B2, an area detector and a laser oscillator are used to confirm the position of the sample mounted on the diffractometer. After roughly adjusting the sample position with the laser beam, the sample is accurately positioned in the center of the diffractometer using a camera. A laser oscillator is installed outside the optical axis (Fig. 1(a)) to prevent inadvertently irradiating white X-rays on

the laser oscillator. Then the sample is irradiated with the laser beam reflected by the mirror installed in the optical axis.

Previously, when the camera was used, the mirror was removed, and the camera was manually placed on the optical axis. The combined use of the laser oscillator and camera was very helpful in adjusting the sample position. However, the position reproducibility of the camera and the mirror was problematic. Additionally, a person had to enter the hutch to change the device position.

In FY2019, the arrangement was changed to solve these problems. The camera is now installed downstream of the mirror (Figs. 1(b) and (c) and the X-ray image transmitted through the mirror is acquired. Before the improvement, X-ray images were observed through a 1-mm-thick lead attenuator to protect the camera. After the improvement, even if high-energy X-rays transmitted through the 1-mm-thick lead attenuator

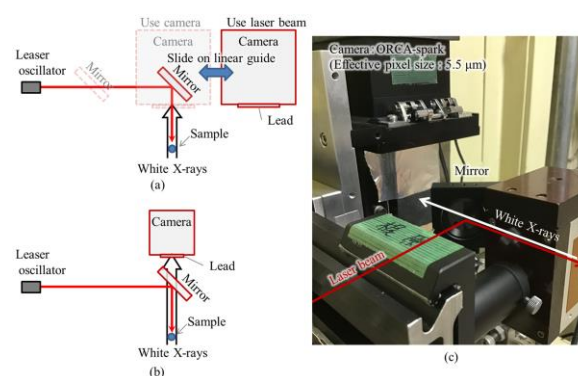


Fig. 1. Camera and laser for sample position confirmation. Schematic of the position (a) before and (b) after the improvement, and (c) a photograph.

further passed through the mirror, the decrease in X-ray intensity is slight. Since the camera and mirror are no longer switched, the reproducibility issue is resolved and there is no need to enter the hutch.

2-2. DXAFS

The higher harmonics elimination mirror used in the DXAFS cut off all or part of the X-rays reflected by the upstream multilayer mirror and the large-sized white X-ray beam. Therefore, the entire mirror chamber had to be removed horizontally from the beam axis to conduct experiments using these X-rays. In addition, the higher harmonic elimination mirror and the position adjusting mechanism were housed in the He flow chamber. However, recent helium supply problems have necessitated improvements to the mirror system to minimize the use of helium gas.

In FY2019, the mirror system was improved (Fig. 2(a)). The mirror chamber was replaced with a vacuum chamber to eliminate the consumption of helium gas. Figures 2(b) and (c) show the evacuation mode of the mirror. The movable range of the adjustment mechanism in the height direction was expanded to allow white X-rays to pass to the downstream hutch without breaking the vacuum in the mirror chamber. In addition, the reflected X-rays

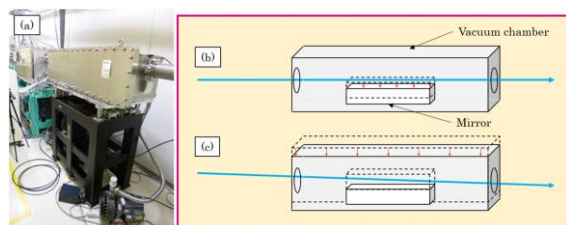


Fig. 2. (a) Higher harmonics-rejecting mirror system and schematic of the evacuation mode for (b) white X-rays and (c) the reflected X-rays of the multilayer mirror.

of the multilayer mirror can also be used by lowering the entire chamber downward via the height adjustment mechanism for the chamber. Consequently, the mirrors can be switched smoothly without breaking the vacuum. In addition, the switching time is greatly reduced.

2-3. High-energy X-ray microtomography

A dedicated X-ray imaging detector for high-energy X-ray microtomography was developed. This is an indirect, visible-light conversion-type X-ray detector. The incident high-energy X-rays onto the scintillator are converted into visible light. The scintillating material is a $\text{Lu}_3\text{Al}_5\text{O}_{12}:\text{Ce}^+$ (LuAG) single crystal or ceramics. The visible-light image is focused on a high-definition CMOS camera (C13949-50U, $4096\text{ (H)} \times 3008\text{ (V)}$ pixels, $3.45\text{ }\mu\text{m} \times 3.45\text{ }\mu\text{m}/\text{pixel}$, 12-bit ADC, Hamamatsu Photonics) by a relay tandem-lens system. In this detector, a large-format lens (Planar 135/3.5, Carl Zeiss) for a large-format camera is used as the first lens to implement a horizontal field of view up to 50 mm, which allows large-sized fossil samples to be observed. By replacing the second lens, the effective pixel size can be changed. To avoid high-energy X-rays entering the CMOS device directly and to reduce the scattered X-rays from a prism mirror, an “L-shaped” optical configuration in the horizontal plane is employed.

Figure 3 shows the exterior and interior views of the detector. The second lens shown in the figure is a camera lens with a focal length of 35 mm. In this case, the effective pixel size of the detector is $12.98\text{ }\mu\text{m} \times 12.98\text{ }\mu\text{m}$. The efficiency and the modulation transfer function were evaluated in scintillators with different thicknesses and materials prior to X-ray microtomography. The evaluation revealed that the

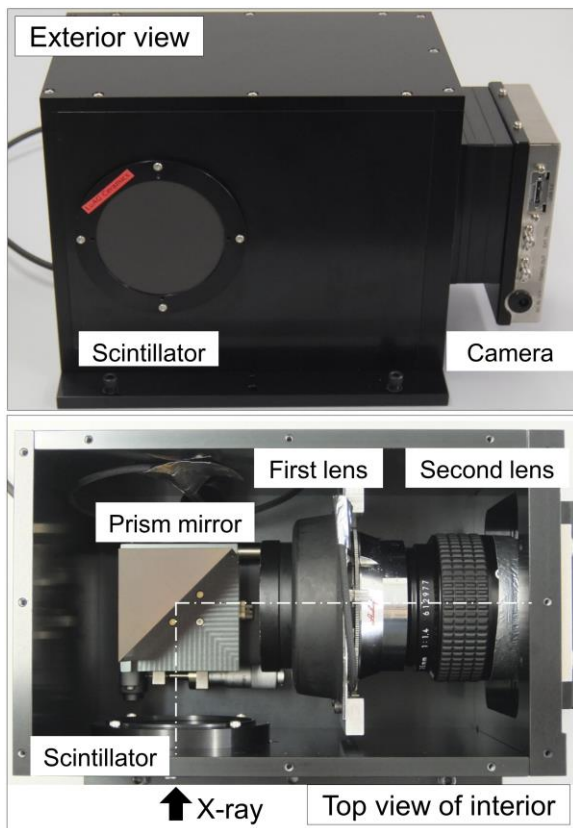


Fig. 3. Exterior and interior of the X-ray detector for wide field of view imaging.

LuAG ceramics with a thickness of 500 μm is suitable for the effective pixel size shown above [1].

As a demonstration of X-ray microtomography with a wide field of view, an elliptical nodule was measured as a fossil sample. Figure 4(a) shows a photograph of the nodule. In this measurement, the distance between the nodule and the detector was set to 3 m. Then, the effective pixel size at the sample position was $12.15 \mu\text{m} \times 12.15 \mu\text{m}$ because the projection image was slightly magnified by the long propagation distance from the sample to the detector. Hence, the horizontal field of view in the projection image was 49.8 mm. The number of projections was 7200 and the exposure time was 25 msec. Since the effective beam size along the vertical direction in the 200-

keV region was less than 2 mm, the nodule was scanned along the vertical direction at 1.42 mm per step to observe the whole shape. Figure 4(b) shows the cross-sectional images in different orthogonal directions. The inside of the nodule and the fossil of a shell indicated by arrows were clearly observed. Figure 4(c) shows the three-dimensional view of the shell. A fossil inclusion was clearly observed with the developed X-ray detector.

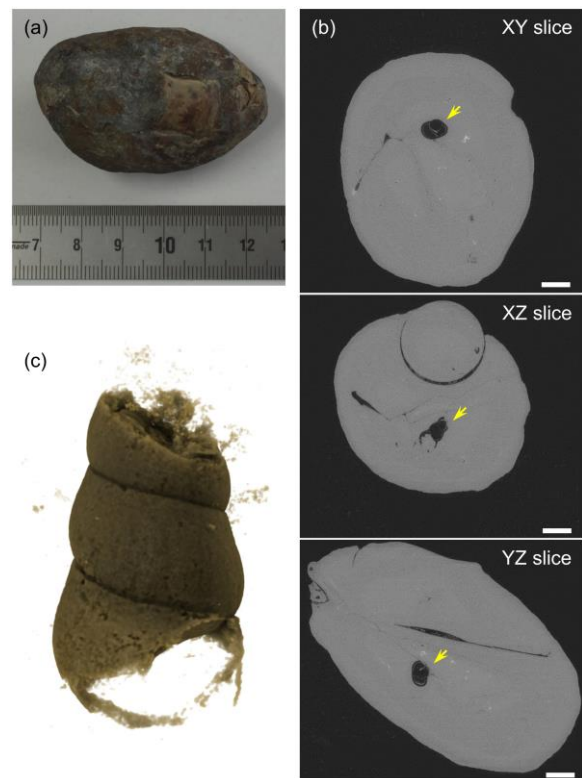


Fig. 4. (a) Photograph of a nodule. (b) X-ray tomographic images of the nodule in XY, XZ, and YZ planes. Scale bar: 5mm. Here, the XY plane is perpendicular to the rotational axis. (c) Three-dimensional view of a fossil inclusion (indicated by the arrows).

Masato Hoshino¹, Keiji Umetani^{*1}, Kazuo Kato^{*1}, and Kentaro Kajiwara^{*2}

*1 Spectroscopy and Imaging Division, Center for Synchrotron Radiation Research, JASRI

*2 Industrial Application Division, diffraction and Scattering Division, Center for Synchrotron Radiation Research, JASRI

Reference:

[1] M. Hoshino, K. Uesugi and N. Yagi, *J. Synchrotron Rad.* **27** (2020) 934-940.